# APPENDIX AVAILABLE ON THE HEI WEB SITE

## Research Report 163

## The Low Emission Zone Baseline Study

**F.J. Kelly et al.**

## Appendix C. Assessing the Oxidative Properties of Ambient $PM_{10}$ and $PM_{2.5}$ Across Greater London

Note: Appendices Available on the Web may appear in a different order than in the original Investigators' Report. HEI has not changed these documents. This appendix was relettered as follows:

**Appendix C was originally Appendix B**

---

Correspondence may be addressed to Dr. Frank J. Kelly, Environmental Health Environmental Research Group, School of Biomedical & Health Sciences, King's College London, 150 Stamford Street, London SE1 9NH, UK *frank.kelly@kcl.ac.uk*

Although this document was produced with partial funding by the United States Environmental Protection Agency under Assistance Award CR–83234701 to the Health Effects Institute, it has not been subjected to the Agency's peer and administrative review and therefore may not necessarily reflect the views of the Agency, and no official endorsement by it should be inferred. The contents of this document also have not been reviewed by private party institutions, including those that support the Health Effects Institute; therefore, it may not reflect the views or policies of these parties, and no endorsement by them should be inferred.

This document was reviewed by the HEI Health Review Committee but did not undergo the HEI scientific editing and production process.

# The London Low Emission Zone Baseline Study

# APPENDIX B

# ASSESSING THE OXIDATIVE PROPERTIES OF AMBIENT $PM_{10}$ AND $PM_{2.5}$ ACROSS GREATER LONDON

## Methods

*Sample collection*

All $PM_{10}$ and $PM_{2.5}$ filters were obtained from Tapered Element Oscillating Microbalance (TEOM) instruments maintained at selected sites throughout the London Air Quality Network, operating in their standard configuration, Air was drawn air through R&P $PM_{10}$ and $PM_{2.5}$sampling inlets at 16.7 L $min^{-1}$. The flow was then split using an isokinetic flow splitter into a main flow of 3 L $min^{-1}$, which passed through the microbalance and an auxiliary flow of 13.7 L $min^{-1}$. The filter and the air stream were heated to 50ºC to reduce the interferences from particle bound water and to minimise thermal expansion of the tapered element that may affect the oscillating frequency.

*Site selection*

Roadside sites were classified as those within one to 5 metres of the kerbside, with sampling heads situated between 2 to 3 meters off the ground, whilst urban background sites were defined as urban locations, away from major traffic sources, which were broadly representative of town/city-wide background concentrations. Within the sites classified as roadside, a panel of sites existed which were located within one metre of the kerb, in this report however we have not elected to subdivide this group further into kerbside (less than one metre) and roadside (more than one and less than 5 metres) locations. The sites were selected to provide a comprehensive geographical coverage of greater London, and to provide contrasts in traffic density and type. Of these 37 sites, 6 of the roadside locations represented the key indicator sites for the assessment of the impact of the introduction of the LEZ: Marylebone Road - Westminster, A206 Cray – Bexley, Westbourne Avenue – Greenwich, Woolwich Flyover – Greenwich, North Circular – Brent, and the Blackwall Tunnel – Tower Hamlets. Provision was also made for filter collection from an additional 'indicator' site at Old Street, Hackney, but at the time of the closure of the current study no ratified filters were available from this site and therefore it is not included in this report. In addition to these sites within the proposed LEZ zone, we also obtained $PM_{10}$ TEOM filters from 4 sites located outside the London conurbation, 2 roadside and 2 background sites located to the north-west and south-east of the city. These sites were selected to provide outside London controls for subsequently assessing the

impact of the LEZ, as well as information on the magnitude of the London-specific increment in $PM_{10}$ oxidative potential.

*$PM_{10}$ filter archive*

All filters analysed in this study were either sent to King's College London via Bureau Veritas or from the local site operatives to King's College London. Masses and a randomised code were assigned to each filter using propitiatory software developed in house, with reflectance determined prior to placing the filters into extraction tubes. Filters were stored in individual non-opaque boxes at r.t.p on receipt at King's College London until determination of reflectance and subsequent extraction, As they had already been heated to 50$^{o}$C in the TEOM and shipped at ambient temperature, it was assumed additional loses of volatile components would be minimal. This view was supported by previous work comparing parallel TEOM and FDMS derived $PM_{10}$ samples, which had indicated no loss of PM oxidative activity in the heated TEOM samples (HEI Report No XXX). The analysts responsible for the extraction of the filters and the subsequent analyses remained blinded to the sample ID for the duration of the study. Samples were extracted and analysed in random order.

*Determination of TEOM filter reflectance*

To assess the darkness of the smoke stains on the TEOM filters, an EEL Model 43 – analogue reflectometer was used (Kemtronix, UK, Ltd, a reference instrument for the EC directive 80/799/EEC for the measurement of smoke stain reflectance). This instrument emits a steady light beam onto the filter surface, which is reflected back from the filter surface to a photosensitive element. The electrical response is then amplified to produce a meter reading, ranging from one to 100% reflectance. Prior to use, the reflectometer was switched on and allowed to warm up for 30 minutes and dust was removed from the surfaces of the white and grey calibration tiles. The measurement head of the reflectometer, fitted with a circular mask, was then placed over the white calibration tile and the reflectance measurement adjusted to 100. The same procedure was then repeated for the grey calibration tile, which provided readings ranging between 34 and 36. This calibration procedure was repeated a number of times until a constant value was obtained for the grey calibration slide, and the pointer returned exactly to 100 with the white calibration surface. The TEOM filters were then placed on a mount situated on a clean

Whatman grade 1 filter paper and the circular mount of the reflectometer head placed over it, taking care to ensure the light beam was focused on the center of the filter surface. The subsequent reflectance reading was then recorded. The reflectance measurement obtained for each filter was then transformed into an absorption coefficient according to ISO 9835 (ISO, 1993) using the formula:

$a=((A/2)/V)\ln(Ro/Rf)$.

In the formula $\alpha$ is the absorption coefficient ($m^{-1}x10^{-5}$); *A*, the loaded filter area ($0.000153m^2$); V, the sampled volume of ambient air ($m^3$); *R*o, the reflectance of field blank filters, and *R*f, the reflectance of the sampled filter (%). The absorption coefficient was multiplied by $10^5$ to yield a more comprehensible number consistent with earlier publications (Cyrys et al, 2003)

*Extraction and re-suspension of TEOM filter PM*

Individual filters, both $PM_{10}$ and $PM_{2.5}$, were placed in 50ml falcon tubes in combination with 2ml of methanol. The tubes were then vortexed for 10 minutes, before sonication using a MSE Soniprep 150 (23kHz) generator, with a titanium probe at an amplitude of 5 microns for 30 seconds on ice. Samples that yielded oily extracts which were not readily resuspended by vortexing, underwent physical scraping from the sides of the extraction tubes with sterile plastic pipettes prior to sonication. The methanol extract was then transferred to a second falcon tube and an additional one ml of methanol added to the remaining filter prior to a further 10-minute period of vortexing. This second methanol extract was then added to the first, prior to drying down under nitrogen at $35^oC$. The dried extract was then re-suspended at a stock concentration of 55.6μg/mL in Chelex100-resin treated ultra-pure water containing 5% HPLC-grade methanol by vortexing for 10 minutes and sonication, as outlined above for 30 seconds at 15 microns. PM extracts were resuspended based on the calculated mass from the TEOM, following ratification of the instrument data. Previous studies have demonstrated good agreement between extracted and measured masses and scanning electron microscopy has been employed to illustrate the efficiency of extractions (HEI Report No XXX).

Contaminating metal concentrations in the water-methanol mixture were reduced by adding 3g of the Chelex-100 resin per 100ml and stirring overnight at $4^oC$. The resin was removed by centrifugation (3,000 rpm for 15 minutes, $4^oC$) and the purified 5% methanol

solution carefully decanted. Prior to use in the resuspension protocol, the pH of the water-methanol solution was adjusted to neutrality using Chelex resin treated 1M hydrochloric acid (HCl) or 1M sodium hydroxide (NaOH). Once PM samples were resuspended in the solution, the pH of the suspension was checked and where necessary readjusted to 7 as outlined above, prior to use in the incubation protocols.

*Ascorbate and urate analysis*

Fifty µl of the PM supernatant was removed and added to 450 µl of ice-cold metaphosphoric acid (MPA) to achieve a final acid concentration of 5%. Ascorbate and urate concentrations were then determined simultaneously using reverse phase HPLC with electrochemical detection. Twenty µL aliquots of each sample were injected for analysis using a Gilson model 231 auto-sampler onto a 10 X 300mm, 5µM C18 column, eluted with 0.2mM Potassium Phosphate buffer ($K_2HPO_4$-$H_3PO_4$), containing 0.25 mM octanesulphonic acid (pH 2.1) at a flow rate of 1ml/min. An EG&G amperometric electrochemical detector (Jones Chromatography, Hengoed, Wales) was used for detection, with E set at 400mV, a time constant of 5s, cathodic output and a sensitivity of 500nA. Sample concentrations were determined against a standard curve of ascorbic acid (0-25µM) and uric acid (0-50µM) (both sigma) prepared in 5% MPA.

*Glutathione analysis*

16.7 µl of the PM supernatants were diluted into 983.3µl of 100mM sodium phosphate buffer, pH 7.5, containing 1mM ethylenediamine tetraacetic acid (EDTA), giving a final pH of around 7. Standards containing 0-165pmol/50µl glutathione disulphide (GSSG), equivalent to 0-330pmol/50µl total glutathione (GSx) were also prepared in the buffer. Fifty µl of sample and standard were then transferred to a microtitre plate wells and 100µl of a reaction mixture was added to each well to give a final concentration in each well of 0.15mM 5, 5'-dithiobis-(2-nitrobenzoic acid) (DTNB), 0.2mM nicotinamide adenine dinucleotide phosphate (NADPH) and 1U of glutathione reductase. Immediately after the addition of the reaction mixture, the microtitre plate was transferred to a plate reader (SpectraMAX 190; Molecular Devices) for analysis. The rate of 5,5′-tetramethylbenzidine (TMB) formation was followed by the rate of change of absorbance at 405nm over a 2 min period at 30°C. To determine GSSG concentration, 5µl of undiluted 2-vinyl pyridine (Aldrich chemical Co, Poole, UK) was added to 130µl of the

samples and standards, vortexed for 5-sec and incubated at room temperature for 1-h. Samples and standards were then plated out and ran as above. The glutathione (GSH) pool was calculated by the subtraction of GSSG (x2) from the total GSx concentration.

*Ascorbate depletion assay*

Oxidative activity of selected PM suspensions was also assessed by their capacity to deplete ascorbate-from an ascorbate only solution. This approach was also used to investigate the mechanisms driving PM oxidative activity, by the addition of the transition metal chelator diethylenetriamine pentaacetic acid (DTPA). To each PM suspension, PM stock solutions were prepared as outlined previously and diluted to a starting concentration of 12.5μg/ml before incubation with ascorbate. All PM exposures were performed in triplicate in UV 96 well flat-bottomed plates (Greiner bio-one) at a final volume of 200 μl. Exposures were initiated by the addition of 20 μl of a concentrated stock of ascorbate (2mM) into each well containing 160 μl of PM suspension. Prior to the addition of the ascorbate to each assay well, the plate was pre-incubated for 10 minutes at 37°C in a plate reader (Spectra Max 190) in the presence or absence of DTPA by the addition of 20 μl of either 2mM DTPA (pH7) or Chelexed water respectively. Final concentrations in the wells were therefore 200 μM of ascorbate, ± of 200 μM DTPA and 10μg/ml of PM.

After addition of ascorbate, the concentration remaining in each well was monitored every 2 minutes for a period of 2 hours by measuring the absorbance at 265nm with the temperature maintained at 37°C. The incubation was limited to 2 hours as evaporative losses were minimal over this period. The rate of ascorbate depletion was determined by performing a linear regression through a concentration verses time plot using the Microsoft Excel 2000 software 'Slope' worksheet function. This was performed for each of the triplicates with the rate of ascorbic acid depletion finally expressed as mean mol $s^{-1}$ x $10^{-9}$ depletion of ascorbate ± standard deviation. In addition to the DTPA treatment, representative PM suspensions were also co-incubated in the presence of a range of inhibitors including the free radical scavengers Cu,Zn-superoxide dismutase and catalase (SOD/CAT), as well as the transition metal chelators EDTA and desferroxamine mesylate (DFO). Similarly to the addition of DTPA, 20 μl of stock solutions of

SOD/CAT (3000 & 1000 U/ml), EDTA (2mM) and DFO (2mM), were added separately to 160 μl of the PM suspensions and pre-incubated as above before addition of 20 μl of the stock ascorbate solution. The final concentrations reached in the incubations were 200 μM ascorbate, 150 & 50 U/ml free radical scavengers (for SOD & CAT respectively), 200 μM EDTA, 200 μM DFO and 10 μg/ml PM. The rate of ascorbate depletion for each treatment was calculated as described above.

*Inductively Coupled Plasma Mass Spectrometry (ICP-MS) analysis of aqueous PM extracts*

One to 2 ml of archived particle suspensions prepared in Chelex100-resin treated ultra-pure water containing 5% HPLC-grade methanol, as outline previously, were centrifuged 13,000 rpm for 1h, 4$^{o}$C to remove particles. To ensure the removal of all particles, the resultant supernatant was filtered through a Anotop-0.02μm Whatman filter. 0.9 ml of the filtrate was then added to a further 0.9 ml of Chelex-100 resin treated HPLC-grade water prior to analysis by ICP-MS. Each batch of samples was ran in parallel to a Chelex-water blank, as well as aqueous extracts derived from ROFA and a stock environmental $PM_{2.5-10}$ sample collected from London, Lambeth Road (collected Aug – Sept 2001). The London sample was ran to provide Fe and Cu measurements, as these metals were low abundance in the aqueous extract obtained from the ROFA sample. Samples were then transferred to the Mass Spectroscopy Unit at King's College London for the quantification of Al, As, Ba, Be, Cd, Cu, Fe,Mn, Mo, Ni, Pb, vV and Zn by ICP-MS using a ELAN DRC ICP-MS (MSF008). Elemental concentrations were determined with reference to a 4-point standard curve based on a ICP multi element standard solution VI CertiPUR® (Merck, Lot. No. OC529648). All concentrations were corrected for the background elemental concentrations, determined in the Chelex-100 resin treated water blank, ran in parallel to each batch of samples.

*Determination of surface mobilisable iron*

Total ($Fe^{2+}$/$Fe^{3+}$) iron concentrations were measured with the use of the chromogenic iron chelator bathophenantroline disulphonate (BPS), which binds specifically to Fe forming a complex that absorbs strongly at 535nm (Nilsson et al. 2002). This characteristic allows for both reduced ($Fe^{2+}$) and total ($Fe^{2+}$/$Fe^{3+}$) iron measurements to be determined

following sample incubation with a reductant (ascorbate). Briefly, 28.2 mg of the $Fe^{2+}$ ion chelator bathophenanthroline disulphonic acid (BPS) was dissolved in 1 ml of deionised $H_2O$ to give a 50 mM stock. Standards of $Fe^{2+}$ (0.1, 0.5, 1, 5, 10, 25 & 50μM) were prepared fresh each day by serial dilution of a 1 mM stock. For preparation of the standard curve, 5 μl of BPS was added to 245 μl of each standard, plus 12.5 μl of a 200 mM ascorbate solution. This standard mixture was then incubated for 30 minutes at room temperature before adding 200 μl of each standard to a 96-well plate and the absorbance read at 535nm against a water blank. Total iron concentrations in PM suspensions were measured in parallel by the addition of 5μl BPS and 12.5μl of 200mM ascorbate (final concentration 9.5mM) to 245μl of sample. This mixture was then incubated for 30 minutes at room temperature after which the PM was removed by centrifugation at 13000 rpm prior to the addition of 200 μl of the resulting supernatant to a 96-well plate where the absorbance was read at 535nm. Blanks were generated by the addition of 17.5 μl of deionised $H_2O$ to 245 μl of each PM suspension, incubating as above, before centrifugation and absorbance measurement. Blank absorbance values were then subtracted from those obtained with the PM samples before the Fe concentrations were calculated from the slope of the standard curve.

**Results**

Figure B1 represents the raw output data from which the oxidative potential (OP) expressions used through this report were derived. Each point represents the mean concentration of a given antioxidant (ascorbate, glutathione and urate) remaining in the synthetic respiratory tract lining fluid (RTLF) following a 4h incubation (37$^{o}$C, pH 7) with 50μg/ml of a given filter extract (both particles with an aerodynamic diameter of 10 μm or smaller [$PM_{10}$] and particles with an aerodynamic diameter of 2.5 μm or smaller [$PM_{2.5}$]). In all cases the starting antioxidant concentrations were 200μM. All samples were incubated in triplicate and the data are summarized as mean concentrations ± 1 standard deviation. The samples are illustrated in the order they were ran, with the data set from the earlier HEI funded study addressing the impact of the introduction of the London Congestion Charging Scheme (CCS) (730 samples) integrated with the data set generated for the Low Emission Zone (LEZ) study (500 samples). The solid black line in each panel illustrates the mean loss of a given antioxidant at 4 h in the particle free

control, the red line that remaining after a 4h incubation with positive control residual oil fly ash sample (50 μg/ml). In both cases these control values represent the mean concentration across all of the 57 batches analyzed in the two studies (36 batched for the CCS and 21 for the LEZ).

These data highlight both the oxidative potential of ambient $PM_{10}$ and $PM_{2.5}$, which often exceeds that associated with the positive control residual oil fly ash (ROFA), as well as the heterogeneity of activity between individual filter extracts examined on an equal mass basis (50 μg/ml). A detailed discussion of these raw output data has previously been presented (HEI Report No. XXX). The key observations at this level of analysis in the current study support these earlier observations and are summarised below:

1. Losses of ascorbate from the RTLF model were in general greater than those observed with glutathione, with a large proportion of the samples yielding greater losses than were observed with ROFA.

2. Whilst a 4-hour incubation with ROFA resulted in a significant loss of ascorbate from the RTLF model, no impact on glutathione was observed, indicting that the soluble metal components of this combustion particle (predominately nickel, vanadium and zinc) (Miller et al 1988) did not catalyze the oxidative consumption of this low molecular weight thiol.

3. As has been reported previously (HEI Report No XXX).  ) a approximate 5-10% loss of total glutathione was seen from the reaction mixtures over the 4 hour incubations period (data not shown). As GSH will only oxidise as far as glutathione disulphide in this model we interpret this finding a being reflective of thiol adsorption to the particle surface, or the formation of GSH conjufates with organic PM components.

4. No loss of urate was noted with any of the ambient or model PM tested consistent with our previous observations (Zielinski et al 1999; Mudway et al 2004; Mudway et al 2005; Kunzli et al 2006).

*Deriving expressions for metal dependant and independent oxidative potential*

In initial experiments we confirmed that DTPA concentrations in excess of 10μM were capable of completely suppressing Fe and Cu-induced losses of ascorbate at concentrations far in excess of those likely to be encountered in our PM suspensions (Figure B2). In addition, DTPA had no impact on the ascorbate depletion observed in this model following incubation with a range of redox cycling quinones: 9,10-phenatroquione, 1,4-naphthoquinone and 1,4-benzoquione (Figure B3). We noted however that the pH of the DTPA solution added to be PM-ascorbate mixture had to be adjusted to 7, or impacts on the rate of quinone catalyzed ascorbate depletion were observed (data not shown). As an alternative strategy, we also examined whether quinones in the PM extracts could be removed, employing an organic extraction protocol using dichloromethane and hexane extraction (1:1), based on a method by Swartz et al. (2003). Whilst this procedure was effective at removing quinone-dependant oxidative activity from aqueous PM extracts, it also resulted in a significant reduction in Cu-induced ascorbate depletion (Figure B4). As this procedure could therefore not be deemed effective at removing quinones without impacting on PM redox active metal content, we elected not to employ the extraction protocol in experiments aimed at establishing the organic radical based oxidative activity in the LEZ PM samples. We thus decided that co-incubation of PM suspensions with a molar excess of DTPA in the ascorbate-only model represented an effective method for isolating the metal dependant component of the total oxidative potential.

Using this approach we analyzed the rate of ascorbate depletion with and without DTPA in all of the $PM_{10}$ and $PM_{2.5}$ samples in the LEZ Baseline study archive to obtain 3 rates: the first indicative of the total oxidative potential, the second, following DTPA treatment, reflecting non metal contributions to the observed activity, and the third, derived from the difference between these two rates, the metal dependant fraction. It should be noted that these experiments were performed at a particle concentration of 10 μg/ml, as opposed to 50 μg/ml to reduce interferences at 263 nm due to the particle suspension. The ascorbate depletion rates for $PM_{10}$ classified by site, within and outside London are illustrated in Figure B5, panel A, with the geographical location of each site illustrated in panel B. As with the oxidative potential measurements made in the full RTLF model, clear site dependent contrasts were observed for total ($P<0.01$ – one-way ANOVA), metal-

dependent (P=0.001) and metal-independent (P<0.01) ascorbate depletion rates, with no clear contrast between roadside and background sites (Figure B5, panel C), or between sites inside or outside of London (Figure B6, panel D). It was notable from this dataset that the majority of the ascorbate dependant oxidative potential was attributable to redox active metals, 68.3±27.5%, though the contribution of metal to the observed activity varied from 0-100% across the whole dataset. As with the $OP^{AA}$/μg measurements in the full RTLF model, site contrasts were apparent in $PM_{2.5}$ total (P=0.001) and metal dependent (P=0.001) ascorbate depletion rates (Figure B6). No site contrasts were however noted in metal independent ascorbate depletion rates (P=0.32). When these data were grouped by site classification, some evidence of enhanced total and metal dependent ascorbate depletion rates were observed at the single urban back ground site in Bloomsbury (BL0) (Figure B6) although as stated previously, observations based on a single background site should be treated with caution. Comparison of the ascorbate depletion rates across the 9 sites that provided both $PM_{10}$ (n=103) and $PM_{2.5}$ (n=94) samples demonstrated comparable total (2.12±1.20 vs. 2.30±1.44 nM/s) and metal dependant rates (2.12±1.20 vs. 1.54±1.48 nM/s). In contrast, the non-metal contribution to the measured rate appeared enhanced in the $PM_{2.5}$ samples (0.58±0.44 vs. 0.76±0.49, P<0.01).

*Soluble and bio-available PM metal composition*

Twelve metals were quantified in aqueous extracts derived from each of the filters: Al, As, Ba, Cd, Cu, Fe, Mn, Mo, Ni, Pb, V and Zn. The $PM_{10}$ metal concentration data, grouped by site are summarized in Figures B7 to B10, with the $PM_{2.5}$ results in Figure B11. As the metal data were not normally distributed, the data has been summarized throughout using median with inter-quartile ranges. A comparison of the determined soluble metal concentrations in $PM_{10}$ samples from roadside (30 sites, 367 samples) and background sites (11 sites, 94 samples) is presented in Figure B12 and illustrates a pattern of differences between the site classifications identical to that reported previously (HEI Report No XXX), with elevated concentrations of Cu, Ba and Mo associated with roadside $PM_{10}$ samples, and Al, As, Cd, Ni, Pb and V concentrations greater at background sites. As with the OP measurements these analyses were repeated using the site means over the study period. These analyses indicated that whilst $PM_{10}$ Cu (P=0.001), Ba (P=0.004) and BPS-Fe (P<0.001) remained enriched at the RS sites, Mo

was no longer significantly different. Similarly of the elements identified as enriched in the UB sites, based on analysis of all filters, only Pb (P=0.05) and V (P=0.01) remained significantly elevated. In contrast, in the $PM_{2.5}$ fraction, no metals were found to be enriched in the roadside samples (8 sites, 82 samples), with the background samples (1 site, 14 samples) containing significantly elevated concentrations of Al, Fe, Pb, V and Zn (Figure B12), suggesting that the enhanced concentrations of Cu, Ba and Mo in the $PM_{10}$ sample was associated with the coarse PM fraction, $PM_{2.5-10}$. This was confirmed by performing a comparison of $PM_{10}$ and $PM_{2.5}$ metal concentrations, which demonstrated an enrichment of Ba, Cu and Mn in the $PM_{10}$ sample (Figure B13).

Due to the low aqueous solubility of Fe, we also examined the content of PM surface mobilisable Fe, using the chromogenic chelator BPS as a ligand. Again the results of this analysis agree well with our previous findings (HEI Report No XXX), with evidence of enhanced BPS-Fe concentrations in $PM_{10}$ samples obtained from roadside sites (Figure B14). A similar roadside enrichment was not apparent in the $PM_{2.5}$ samples (Figure B15), again suggesting that the mobilized Fe pool associated with the coarse mode. BPS-Fe was found to correlate well with $OP^{AA}/\mu g$ ($r=0.26$, $P<0.001$) and $OP^{GSH}/\mu g$ ($r=0.37$,$P<0.001$), Figure B16, but less strongly with the various ascorbate depletion rates: total ($r=0.21$,$P<0.001$), metals dependent ($r=0.18$,$P<0.001$) and metal independent ($r=0.12$,$P<0.05$), Figure B17.

*Filter reflectance*

Filter reflectance was measured as a surrogate for BS (elemental carbon) on all filters prior to extraction. These data were then transformed to absorbance units and multiplied by $10^5$ to make the readings more comprehensible as outlined in the methods section. The final data are presented in Figure B18. A one-way ANOVA of this data set failed to demonstrate any clear site contrast for either $PM_{10}$ or $PM_{2.5}$. However, when the individual filter absorbencies were categorized as roadside and urban background samples, a clear increase in PM absorbance was seen to be associated with roadside sites. Notably, particle absorbance did not appear to be predictive of any of the PM oxidative potential measurement made in the present study (Chapter 2-Table 5).

## References

Kunzli N, Mudway IS, Gotschi T, Shi T, Kelly FJ, Cook S, Burney P, Forsberg B, Gauderman JW, Hazenkamp ME, Heinrich J, Jarvis D, Norback D, Payo-Losa F, Poli A, Sunyer J, Borm PJ. 2006. Comparison of oxidative properties, light absorbance, total and elemental mass concentration of ambient PM2.5 collected at 20 European sites. Environ Health Perspect 114:684-690.

Miller CA, Linak WP, King C, Wendt JOL. 1998. Fine particle emissions from heavy fual oil combustion in a firetube package boiler. Combust Sci and Tech 134:477-502.

Mudway IS, Stenfors N, Duggan ST, Roxborough H, Zielinski H, Marklund SL, Blomberg A, Frew AJ, Sandstrom T, Kelly FJ. 2004. An in vitro and in vivo investigation of the effects of diesel exhaust on human airway lining fluid antioxidants. Arch Biochem Biophys 423:200-212.

Mudway IS, Duggan ST, Venkataraman C, Habib G, Kelly FJ, Grigg J. 2005. Combustion of dried animal dung as biofuel results in the generation of highly redox active fine particulates. Part Fibre Toxicol 4:6

Zielinski H, Mudway IS, Berube KA, Murphy S, Richards R, Kelly FJ. 1999. Modeling the interactions of particulates with epithelial lining fluid antioxidants. Am J Physiol 277:L719-L726.

## Abbreviations

| | |
|---|---|
| CCS | Congestion Charging Scheme |
| GSSG | glutathione disulphide |
| LEZ | London-wide Low Emission Zone |
| OP | oxidative potential |
| PM | particulate matter |
| $PM_{2.5}$ | particles with an aerodynamic diameter of 2.5 μm or smaller |
| $PM_{10}$ | particles with an aerodynamic diameter of 10 μm or smaller |
| ROFA | residual oil fly ash |
| RTLF | respiratory tract lining fluid |

## Figure Legends

Figure B1: Raw output data from which the oxidative potential (OP) expressions used in Chapter 2 were derived. 500 TEOM filters (358 $PM_{10}$ and 142 $PM_{2.5}$), run in 21 batches,

were extracted and the recovered PM analyzed for their capacity to deplete ascorbate, urate and glutathione from a synthetic RTLF. Each point represents the mean concentration of a given antioxidant remaining in the synthetic RTLF following a 4h incubation (37$^{o}$C, pH 7) with 50μg/ml of a given filter extract (both particles with an aerodynamic diameter of 10 μm or smaller [$PM_{10}$] and particles with an aerodynamic diameter of 2.5 μm or smaller [$PM_{2.5}$]). In all cases the starting antioxidant concentrations were 200μM. All samples were incubated in triplicate and the data are summarized as mean concentrations ± 1 standard deviation.

Figure B2: Inhibition of ascorbate depletion by the redox active metals Fe (10μM) and Cu (10μM) in the presence of increasing concentrations of the metal chelator DTPA. All data represent the mean (SD) of triplicate incubations.

Figure B3: Inhibition of ascorbate depletion by the redox active metals Fe (10μM) and Cu (10μM), as well as the redox-cycling quinones 9,10-phenatroquione (PQ – 1μM), 1,4 naphthoquinone (NQ – 1μM) and 1,4-benzoquione (BQ 1-μM) with the addition of the metal chelator DTPA (final concentration 200μM). All data represent the mean (SD) of triplicate incubations.

Figure B4: Inhibition of ascorbate depletion by the redox active metals Fe (10μM) and Cu (10μM), as well as the redox-cycling quinones 9,10-phenatroquione (PQ – 1μM), 1,4 naphthoquinone (NQ – 1μM) and 1,4-benzoquione (BQ 1-μM) following extraction of the quinone compounds from the aqueous phase into an organic phase of dichloromethane and hexane (1:1). Extraction was achieved by mixing 3ml of the metal/quinone solutions with 3ml of the extraction mixture for 5 minutes. After this period of sample agitation the phases were separated by centrifugation at3,000 rpm for 10 minutes (4$^{o}$C) and the organic phase removed. The remaining aqueous phase was then used in the ascorbate depletion assay. All data represent the mean (SD) of triplicate incubations.

Figure B5: Panel A illustrates the mean ± 1 standard deviation total (orange bars, from baseline) and metal independent (yellow bars, from baseline) $PM_{10}$ ascorbate depletion

rates (37$^{o}$C, pH7) for each of the 41 sites studied in the current analysis, with panel B illustrating the geographical location of the sites within and outside London. The metal dependent ascorbate depletion rate is reflected by the difference in the means between the total and metal independent rates. Sites are grouped to illustrate whether they are located within central London, or fall outside to the metropolitan area, with site codes in black text reflecting roadside and blue text urban background sites. The number of filer samples in each group is given in Tables 1 and 2. Panel C illustrates the oxidative potential of all roadside (RS) vs., background (UB) sites, with the total rate, split into metal dependent and independent fractions. In panel D samples derived from RS and UB sites are grouped to illustrate whether the site is located within central London, or falls outside to the metropolitan area, with orange bars reflecting roadside and yellow bars urban background sites. Comparison of rates between the two site classifications and between inner and outside London sites were performed using a 2-tailed unpaired T-test, assuming unequal group variances. NS = a non-significant difference.

Figure B6: Mean ± 1 standard deviation total (orange bars, from baseline) and metal independent (yellow bars, from baseline) ascorbate depletion rates (37$^{o}$C, pH7) for the 9 sites from which $PM_{2.5}$ samples were obtained. The metal dependent ascorbate depletion rate is reflected by the difference in the means between the total and metal independent rates. Roadside site codes are in black text reflecting roadside whilst urban background site codes are represented. The number of filer samples in each group is given in Table 1. The upper panel illustrates the oxidative potential of all roadside (RS) vs., background (UB) sites, with the total rate, split into metal dependent and independent fractions. Comparison of rates between the two site classifications was performed using a 2-tailed unpaired T-test, assuming unequal group variances. NS = a non-significant difference, *$p<0.05$, **$p<0.01$.

Figure B7: Data are illustrated as box plots, with the central line reflecting the median, the extreme borders of the box, the inter-quartile range and the whiskers the 95% confidence intervals. Samples are grouped to illustrate whether the site is located within central London, or falls outside to the metropolitan area, with orange bars reflecting

roadside and yellow bars urban background locations. The number of filer samples in each group is given in Table 1.

Figure B8: All details are as outlined in figure B7.

Figure B9: All details are as outlined in figure B7.

Figure B10: All details are as outlined in figure B7.

Figure B11: Data are illustrated as box plots, with the central line reflecting the median, the extreme borders of the box, the inter-quartile range and the whiskers the 95% confidence intervals. Roadside sites are illustrated with orange bars, whilst the single urban background site (BL0) is represented as a yellow bar. The number of filer samples in each group is given in Table 1.

Figure B12: Water-soluble metal concentrations associated with $PM_{10}$ and $PM_{2.5}$ samples from the sites highlighted in Figures B7-B11, classified according the roadside (orange bars, n=367) or urban background (yellow bars, 94) designation. Data are illustrated as box plots, with the central line reflecting the median, the extreme borders of the box, the inter-quartile range and the whiskers the 95% confidence intervals. Comparison of metal concentrations between RS and UB sites was performed using the Mann-Whitney test for non-parametric data. Where the results of these analyses have revealed a significant difference in a specific metal, where the concentration is higher in the RS than UB samples, the level of significance (*$p<0.05$, **$p<0.01$, ***$p<0.001$) is illustrated in blue. Conversely where the higher metal concentration id associated with the UB samples the level of significance is illustrated in black.

Figure B13: Water-soluble metal concentrations associated with $PM_{10}$ (orange bars) and $PM_{2.5}$ (red bars) from the sites highlighted in Figures B7-B11, classified by PM fraction, ($PM_{10}$, n=461 and $PM_{2.5}$, n=96). Roadside and urban background sites have been grouped in this analysis. Data are illustrated as box plots, with the central line reflecting the median, the extreme borders of the box, the inter-quartile range and the whiskers the 95% confidence intervals. Comparison of metal concentrations between fractions was

performed using the Mann-Whitney U test for non-parametric data. Where the results of these analyses have revealed a significant difference in a specific metal, where the concentration is higher in $PM_{10}$, the level of significance (*p<0.05, **p<0.01, ***p<0.001) is illustrated in blue. Conversely where concentrations are higher in $PM_{2.5}$ the level of significance is illustrated in black.

Figure B14: Site data are illustrated as box plots, with the central line reflecting the median, the extreme borders of the box, the inter-quartile range and the whiskers the 95% confidence intervals. Samples are grouped to illustrate whether the site is located within central London, or falls outside to the metropolitan area, with orange bars reflecting roadside and yellow bars urban background sites. The number of filer samples in each group is given in Table 1. The right hand panels illustrates the median BPS-total Fe concentrations associated with all roadside (RS) and background (UB) site filters. Comparison BPS-Fe at RS and UB sites was performed using the Mann-Whitney U test for non-parametric data, ***p<0.001.

Figure B15: All details are as outlined in Figure B14.

Figure B16: Details of the linear regressions through each of these data sets are illustrated.

Figure B17: Details of the linear regressions through each of these data sets are illustrated.

Figure B18: Mean ± 1 standard deviation ascorbate $PM_{10}$ and $PM_{2.5}$ absorbance for each of the 41 sites studied in the current analysis. Absorbance was derived from raw reflectance data as outlined in the methods. Samples are grouped to illustrate whether the site is located within central London, or falls outside to the metropolitan area, with orange bars reflecting roadside and yellow bars urban background sites. The number of filer samples in each group is given in Table 1. The right hand panels illustrate the oxidative potential of all roadside and background $PM_{10}$ and $PM_{2.5}$ filters, with comparison between the two site classifications performed using a 2-tailed unpaired T-

test, assuming unequal group variances. NS = a non-significant difference, *** that a comparison of OP between the groups yielded a p-value <0.001.

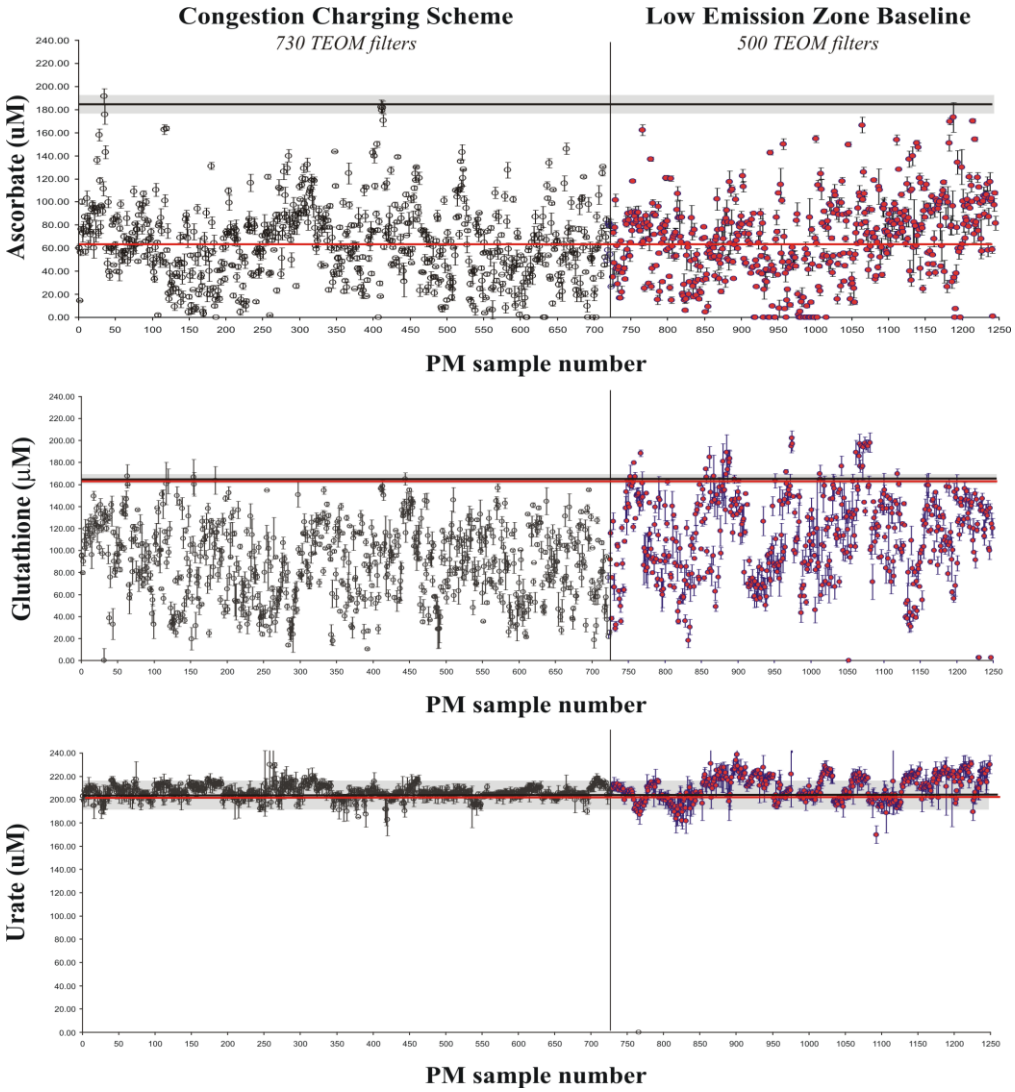


Figure B1. Summary of antioxidant depletion rates across the CCS and LEZ baseline projects.

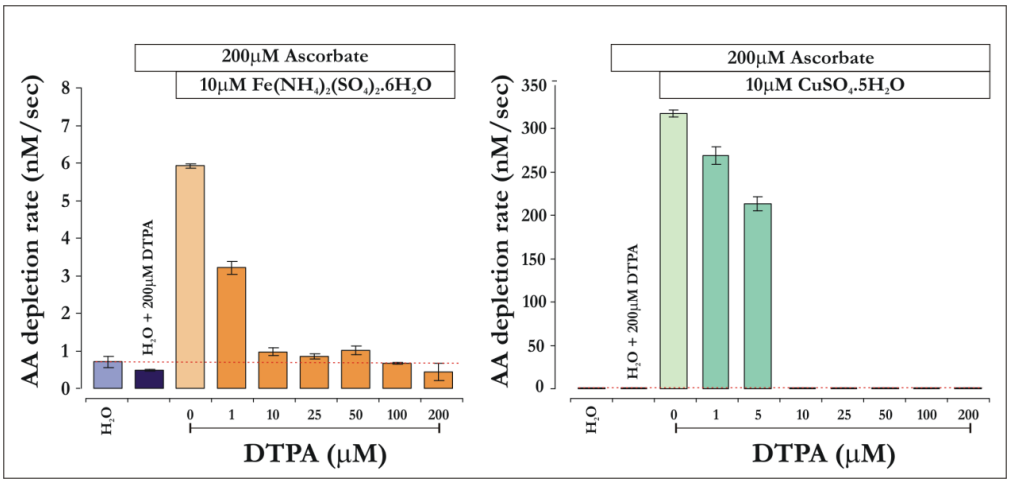


Figure B2. Inhibition of ascorbate depletion by metal chelation with DTPA.

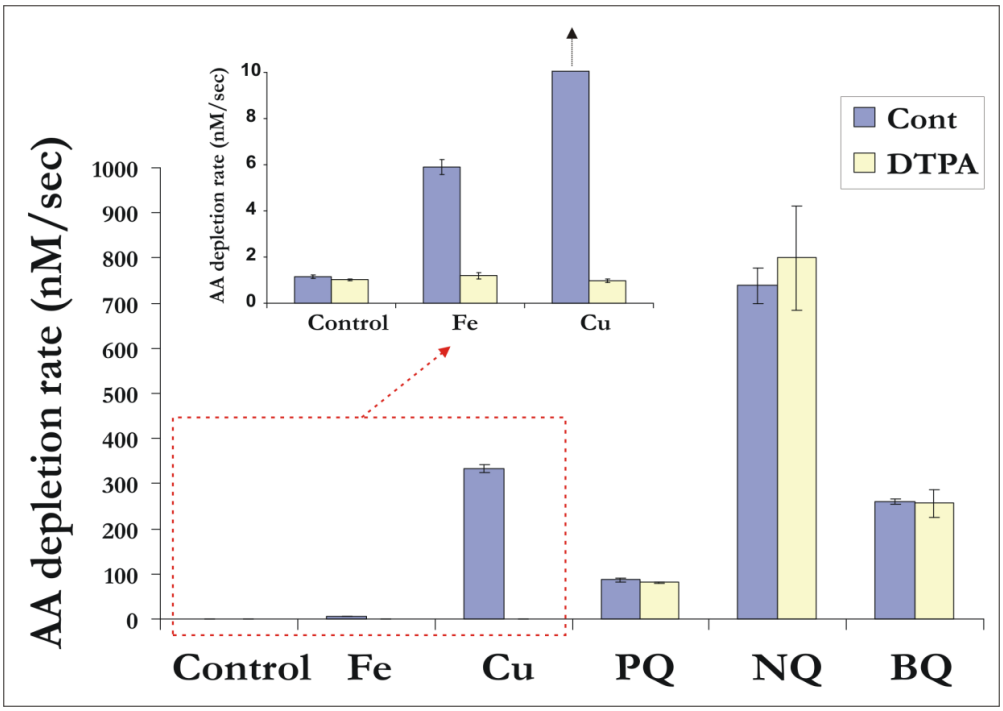


Figure B3. Inhibition of ascorbate depletion by Fe and Cu, as well as 9,10-phenatroquione, 1,4 naphthoquinone and 1,4-benzoquione with the metal chelator DPTA.

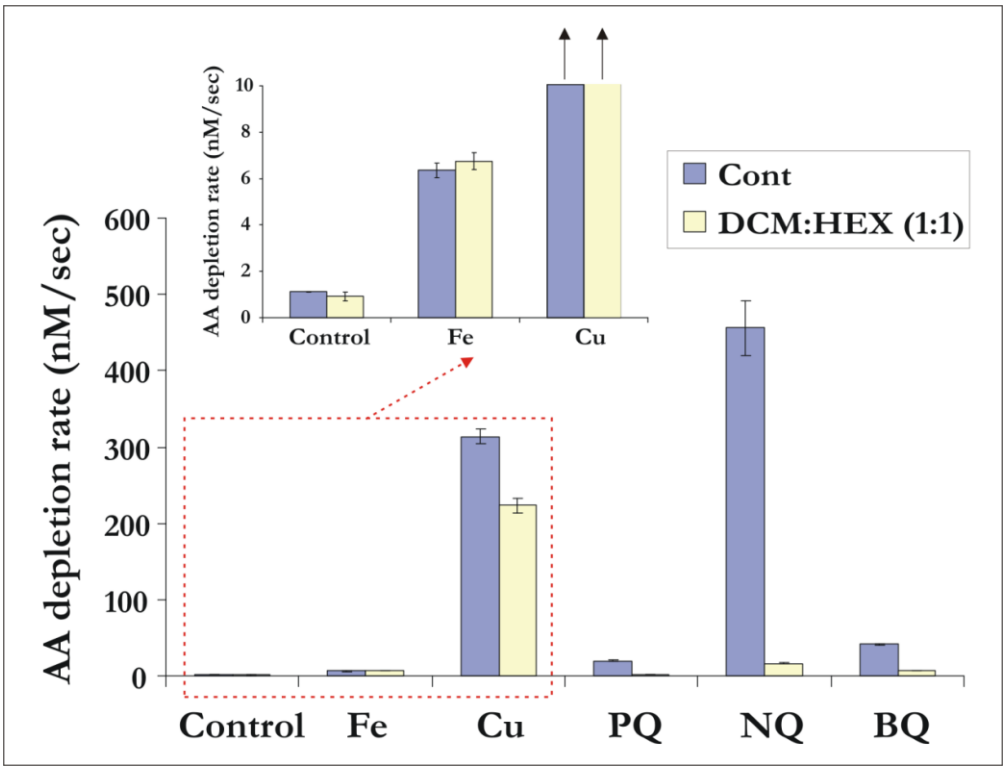


Figure B4. Inhibition of ascorbate depletion by Fe and Cu (10μM), as well as the quinones 9,10-phenatroquione, 1,4 naphthoquinone and 1,4-benzoquione following extraction of the quinone compounds.

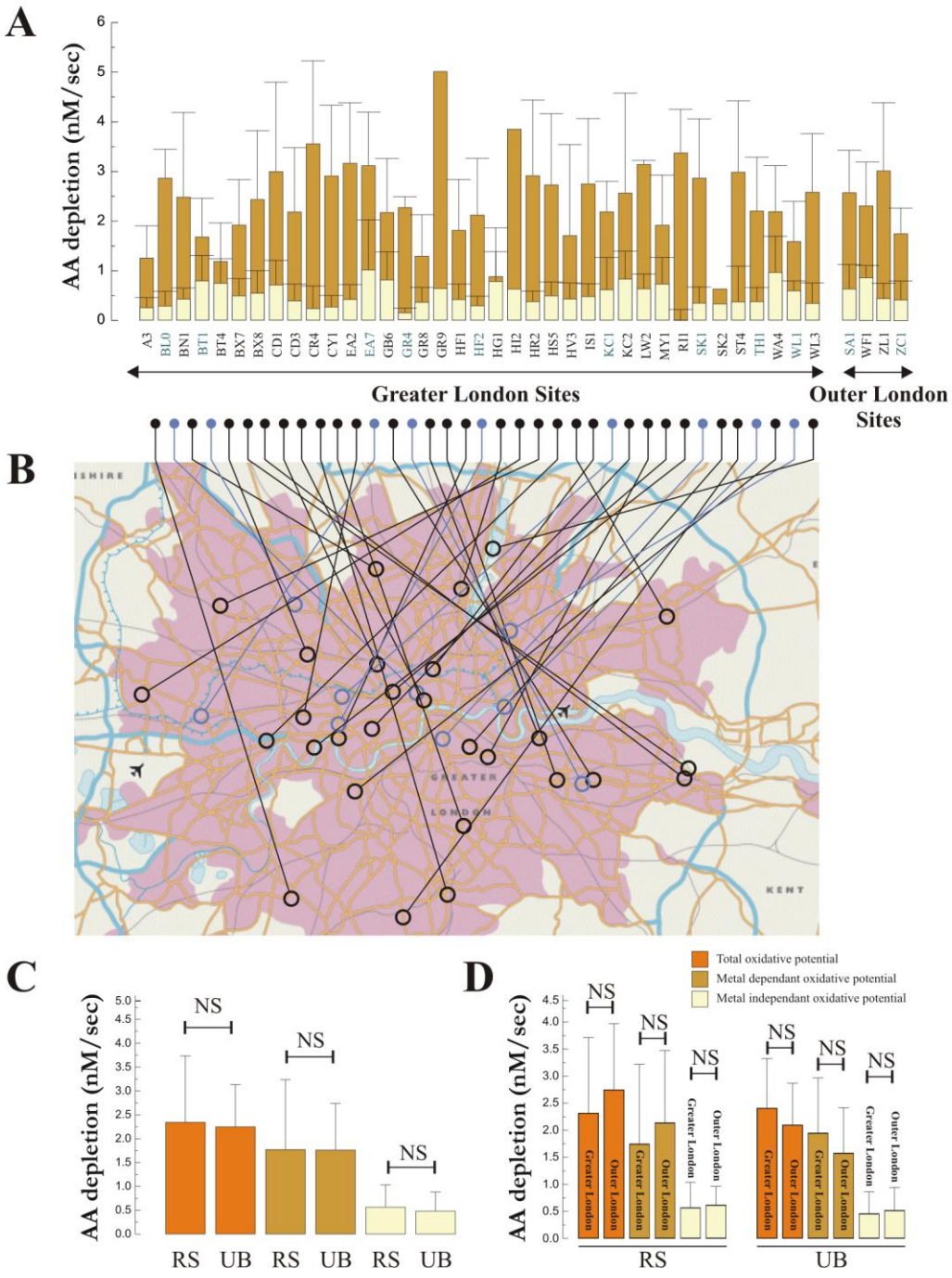


Figure B5. Metal-dependant and –independent ascorbate depletion across $PM_{10}$ London sites.

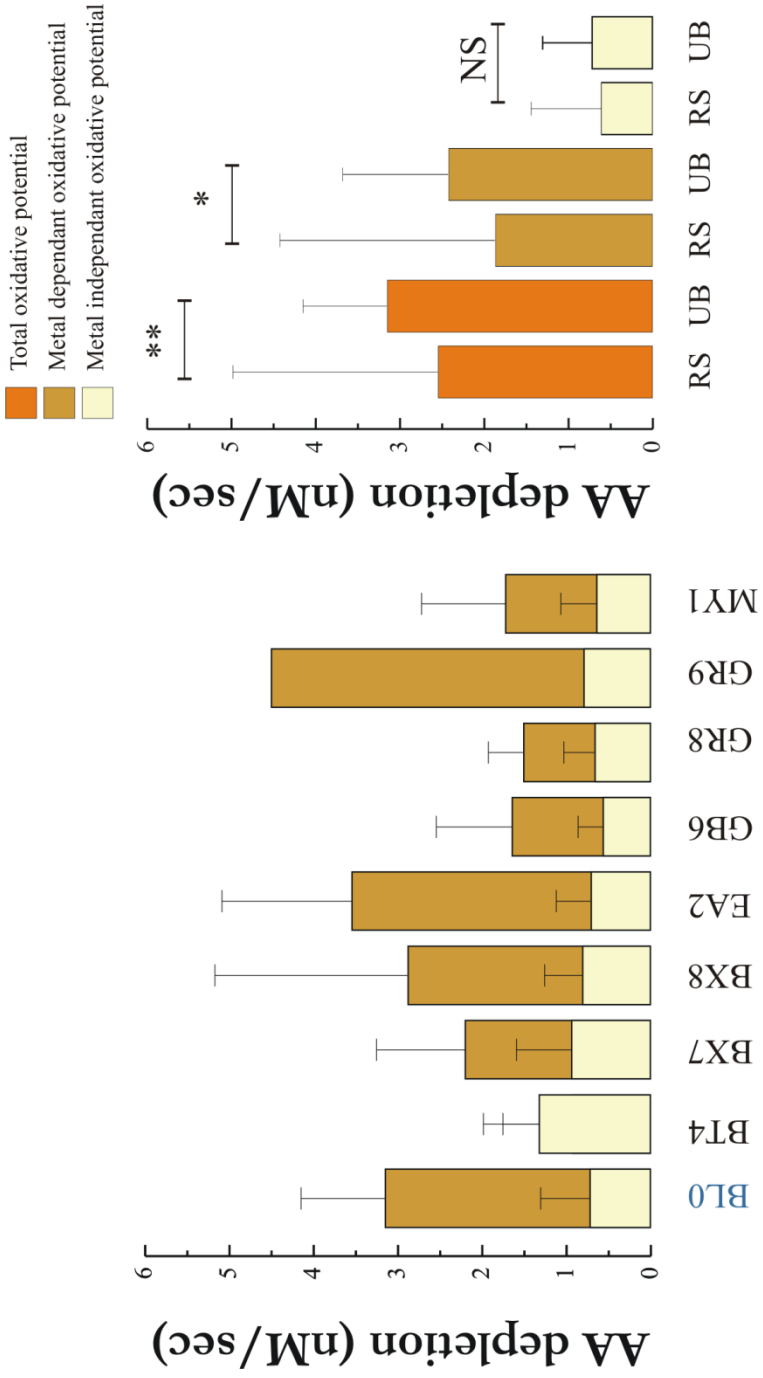


Figure B6. Metal-dependant and –independent ascorbate depletion across $PM_{2.5}$ London sites.

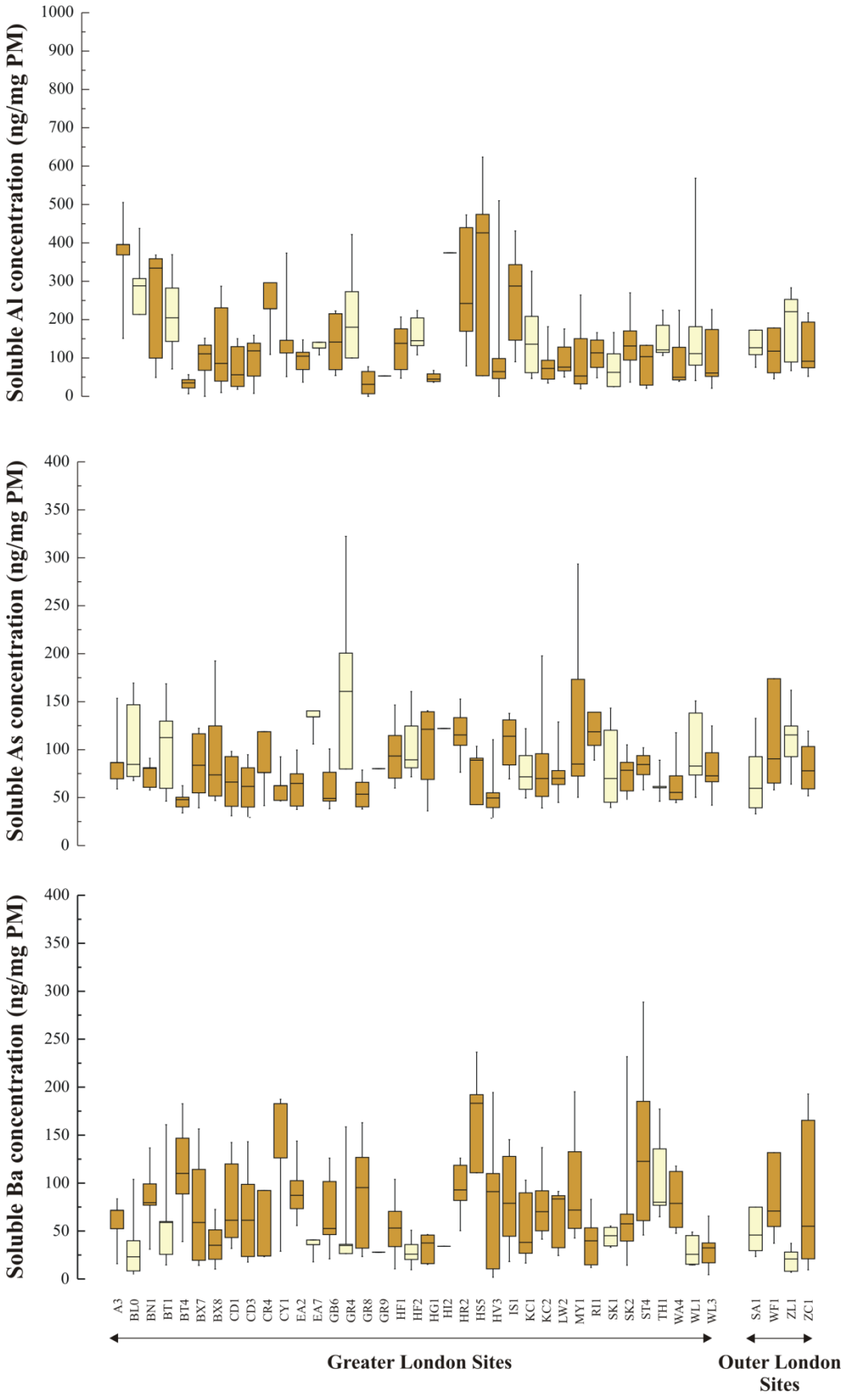
Soluble Al concentration (ng/mg PM)
1000
900
800
700
600
500
400
300
200
100
0
Soluble As concentration (ng/mg PM)
400
350
300
250
200
150
100
50
0
Soluble Ba concentration (ng/mg PM)
400
350
300
250
200
150
100
50
0
A3
BL0
BN1
BT1
BT4
BX7
BX8
CD1
CD3
CR4
CY1
EA2
EA7
GB6
GR4
GR8
GR9
HF1
HF2
HG1
HI2
HR2
HS5
HV3
IS1
KC1
KC2
LW2
MY1
RI1
SK1
SK2
ST4
TH1
WA4
WL1
WL3
SA1
WF1
ZL1
ZC1
Greater London Sites
Outer London Sites

Figure B7. Water-soluble Al, As and Ba concentrations associated with $PM_{10}$ samples obtained from each of the designated sites.

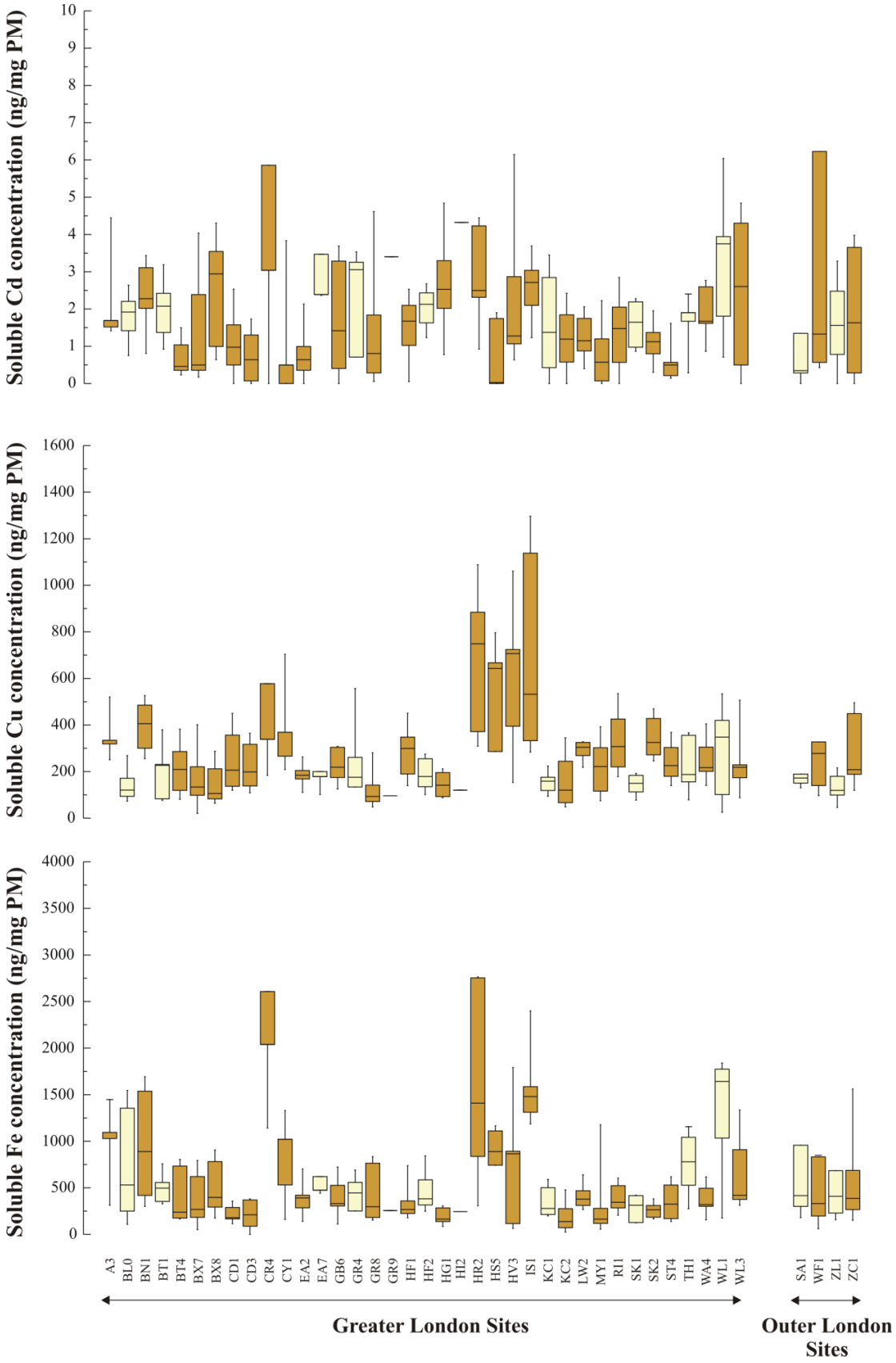

Figure B8. Water-soluble Cd, Cu and Fe concentrations associated with $PM_{10}$ samples obtained from each of the designated sites.

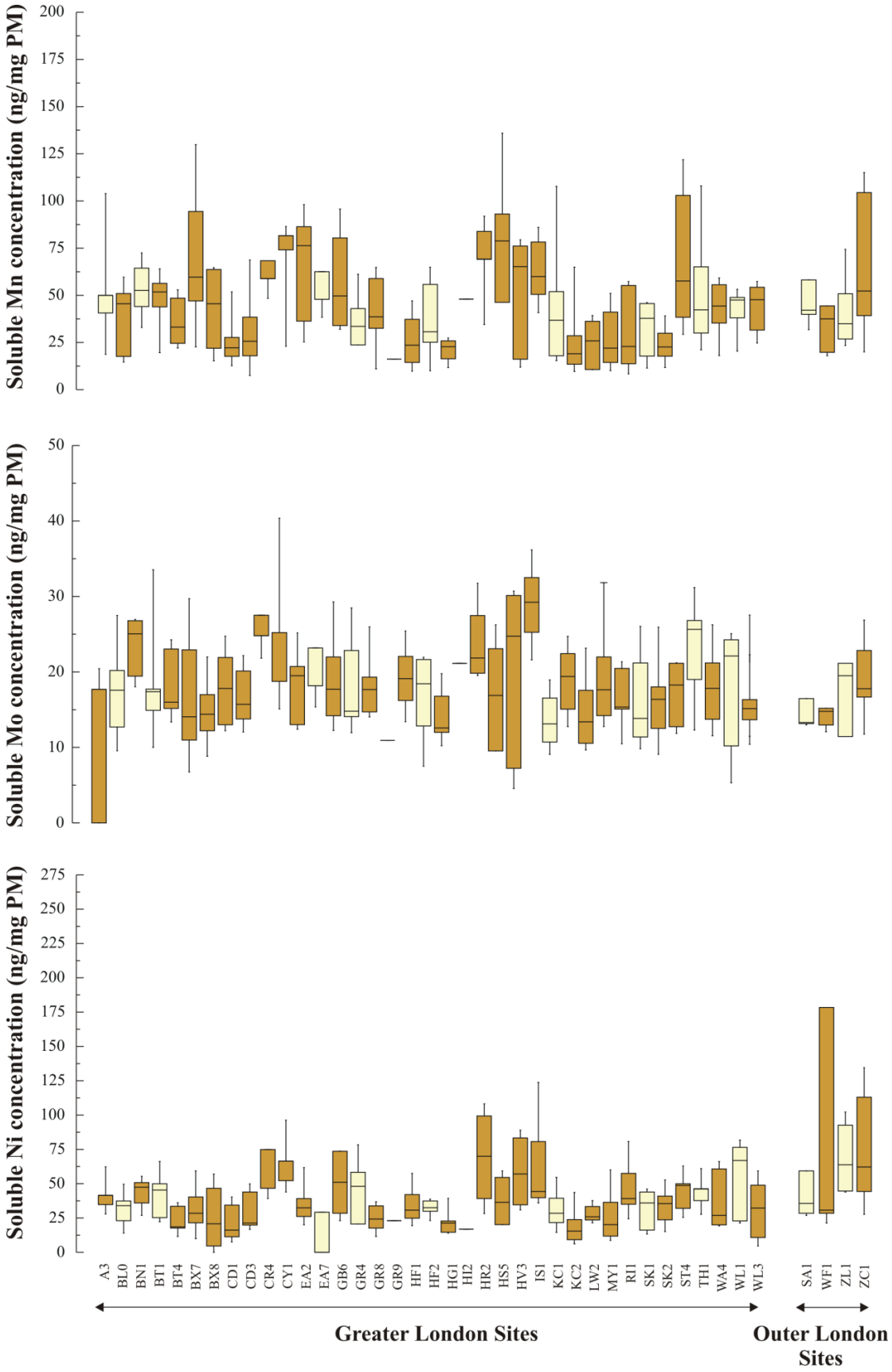


Figure B9. Water-soluble Mn, Mo and Ni concentrations associated with $PM_{10}$ samples obtained from each of the designated sites.

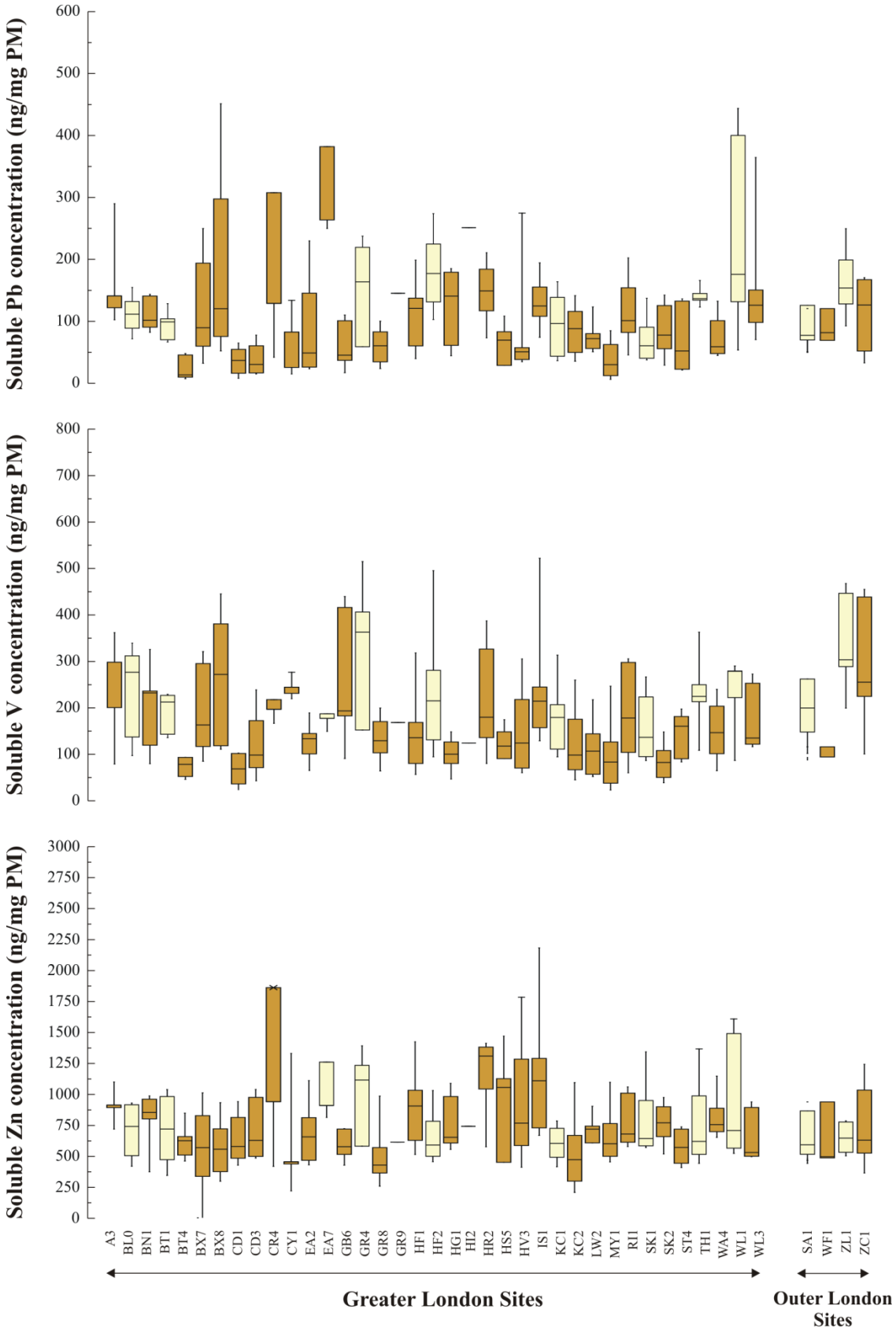
Soluble Pb concentration (ng/mg PM)
600
500
400
300
200
100
0
Soluble V concentration (ng/mg PM)
800
700
600
500
400
300
200
100
0
Soluble Zn concentration (ng/mg PM)
3000
2750
2500
2250
2000
1750
1500
1250
1000
750
500
250
0
A3
BL0
BN1
BT1
BT4
BX7
BX8
CD1
CD3
CR4
CY1
EA2
EA7
GB6
GR4
GR8
GR9
HF1
HF2
HG1
HI2
HR2
HS5
HV3
IS1
KC1
KC2
LW2
MY1
RI1
SK1
SK2
ST4
TH1
WA4
WL1
WL3
SA1
WF1
ZL1
ZC1
Greater London Sites
Outer London Sites

Figure B10. Water-soluble Pb, V and Zn concentrations associated with $PM_{10}$ samples obtained from each of the designated sites.

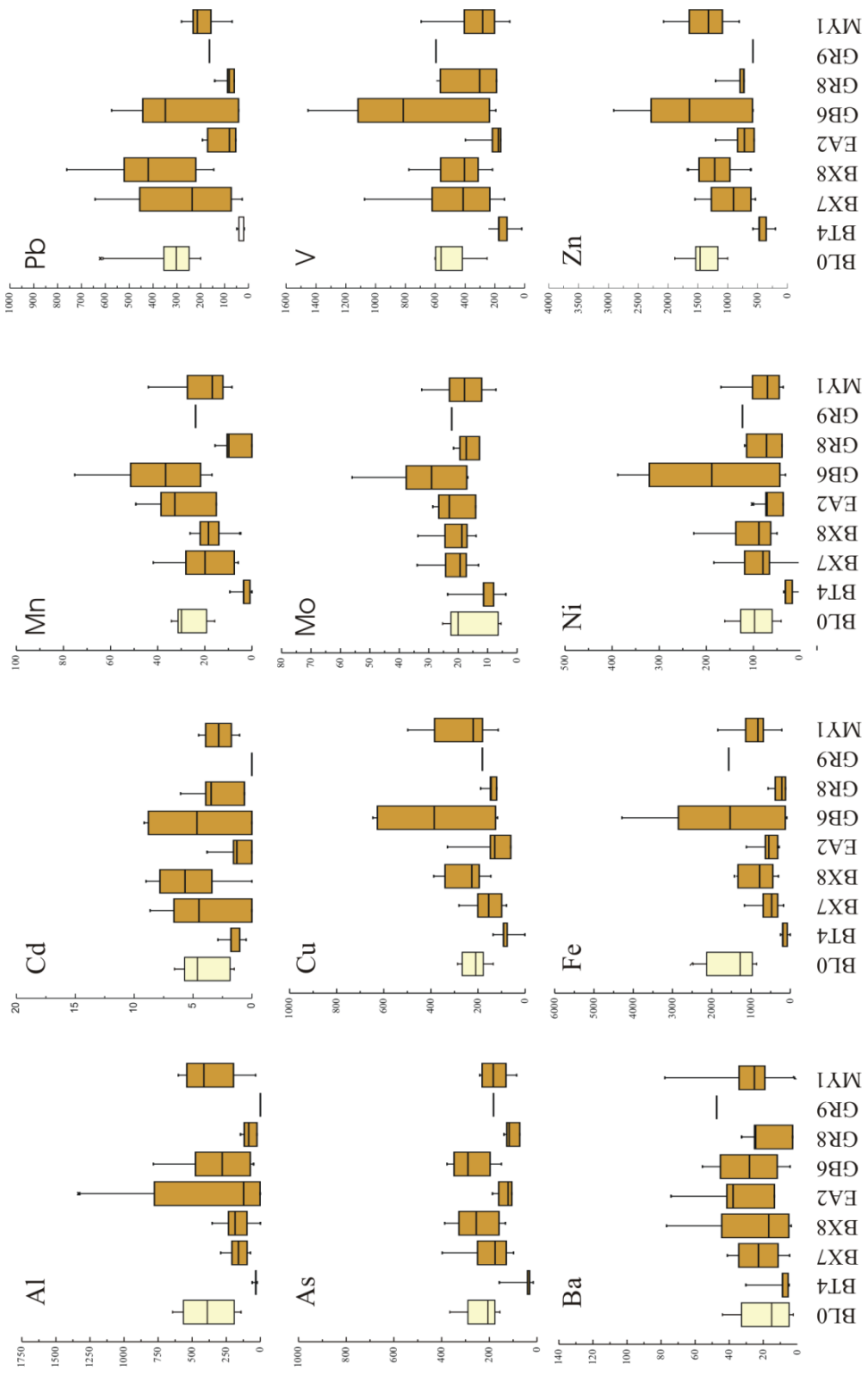


**Soluble metal concentration (ng/mg PM)**

Figure B11. Water-soluble metal concentrations associated with each of the sites from which $PM_{2.5}$ samples were obtained.

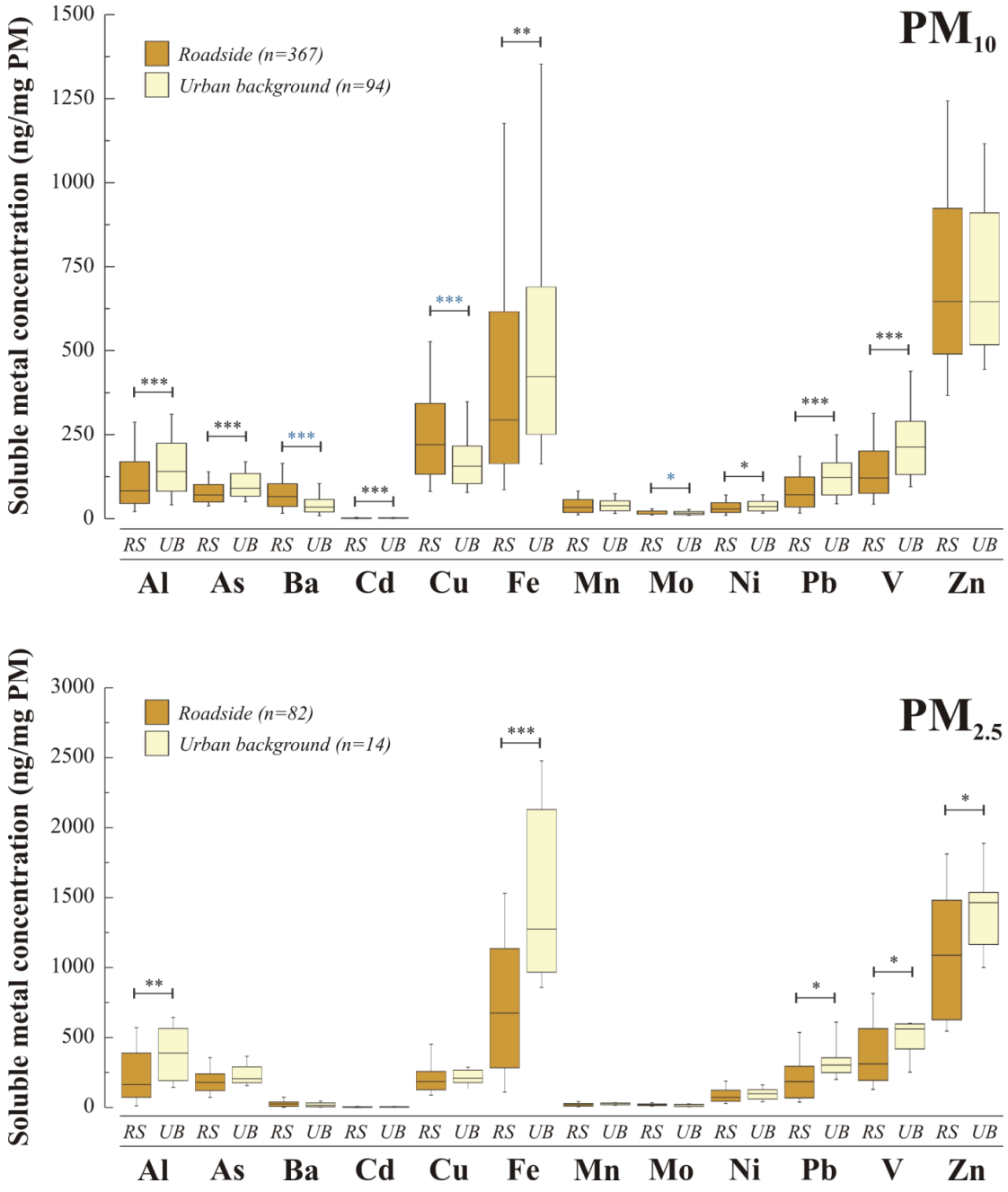


Figure B12. Summary of water-soluble metal concentrations associated with $PM_{10}$ and $PM_{2.5}$ samples.

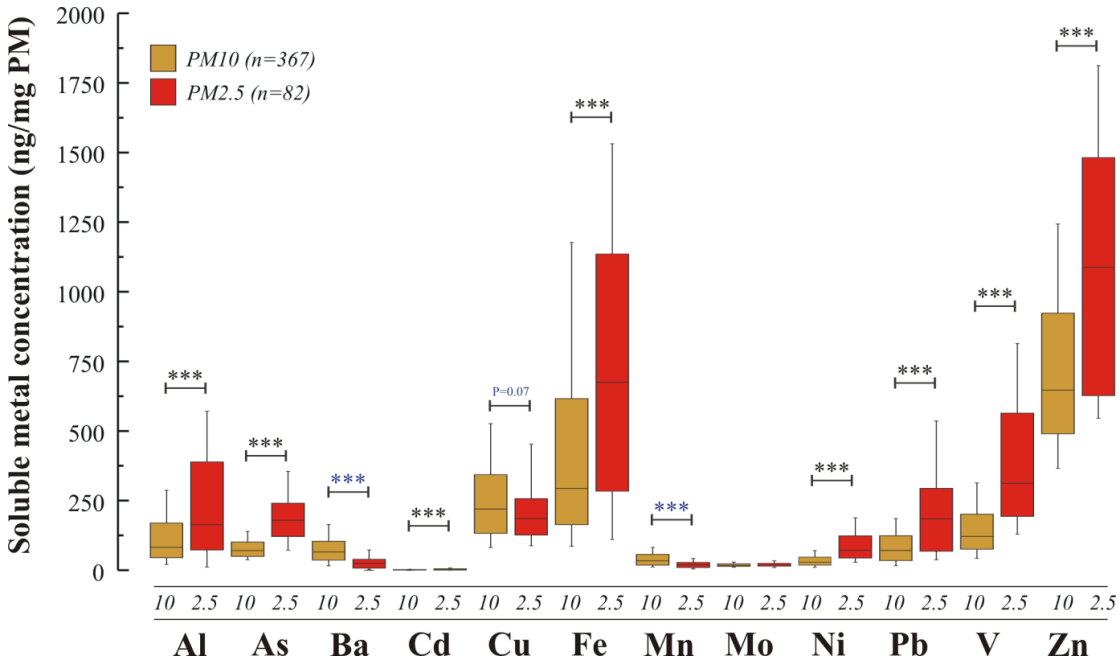


Figure B13. Summary of water-soluble metal concentrations associated with $PM_{10}$ and $PM_{2.5}$.

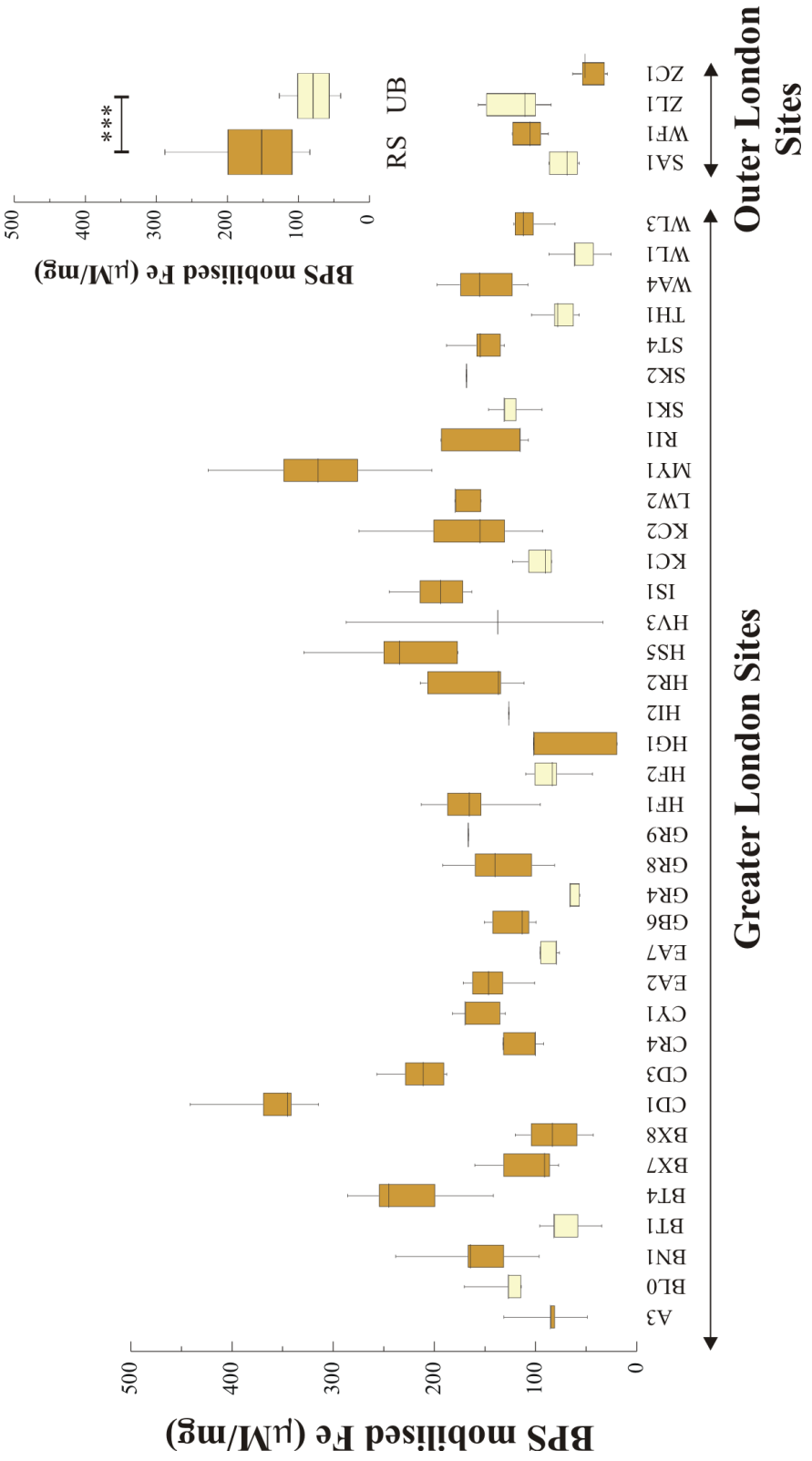


Figure B14. Total ($Fe^{2+}$ + FeIII) BPS mobilised Fe concentrations associated with each of the sites which supplied $PM_{10}$ filters.

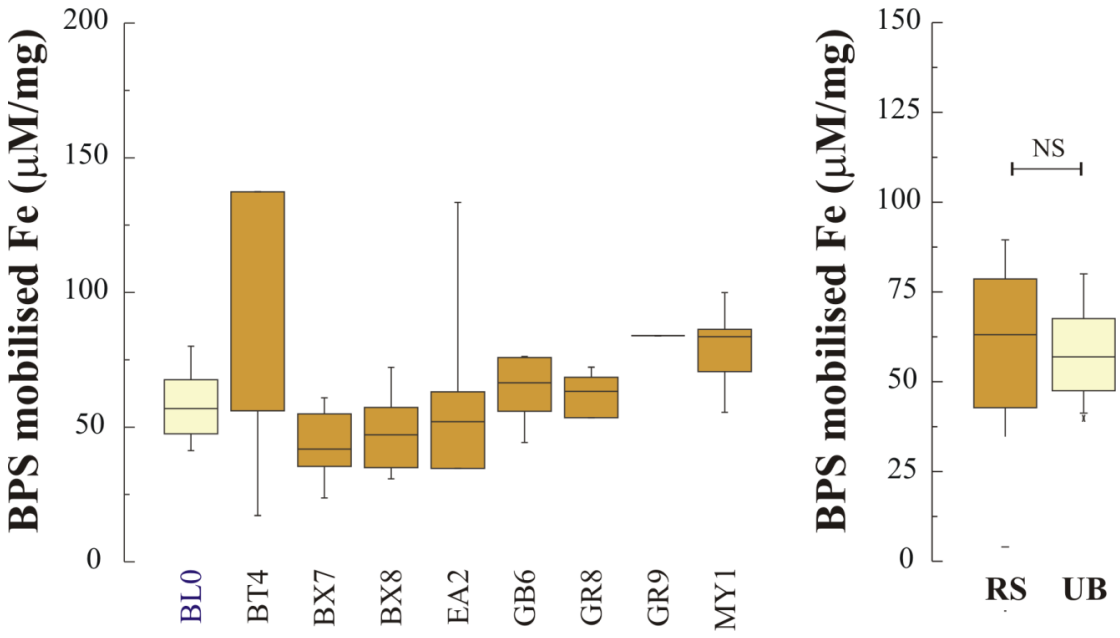


Figure B15. Total ($Fe^{2+}$ + FeIII) BPS mobilised Fe concentrations associated with the sites 9 which supplied $PM_{2.5}$ filters.

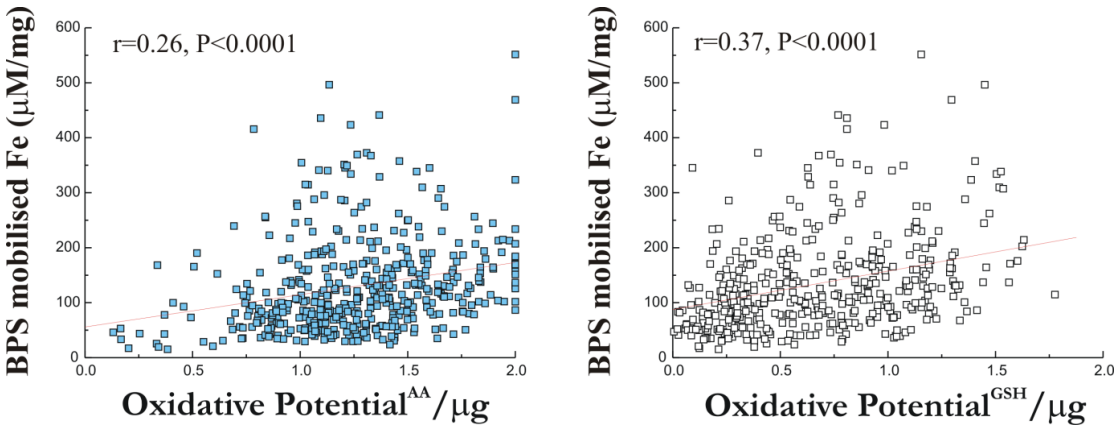


Figure B16. The relationship between ascorbate and glutathione dependant oxidative potential ($OP^{AA}$/μg, $OP^{GSH}$/μg) with BPS total Fe.

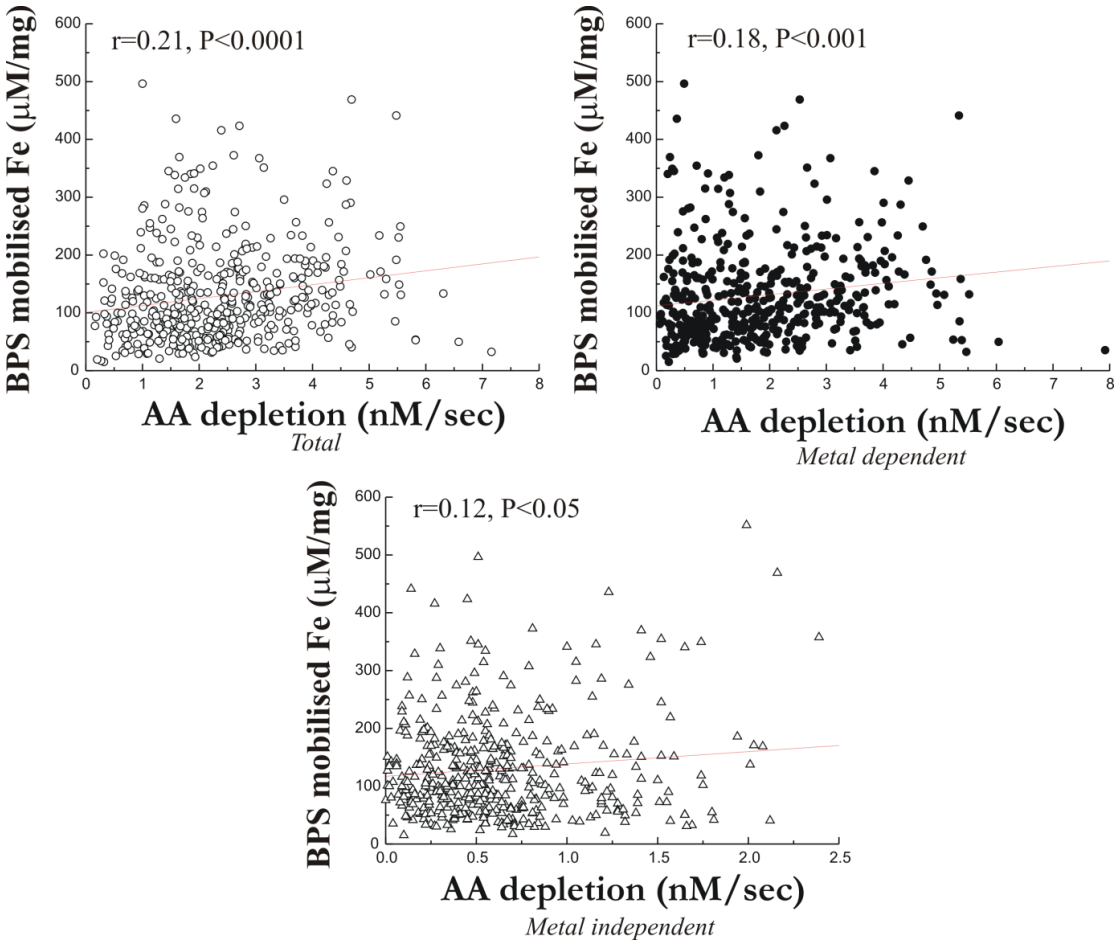


Figure B17. The relationship between total, metal dependent and independent ascorbate depletion rates with BPS total Fe.

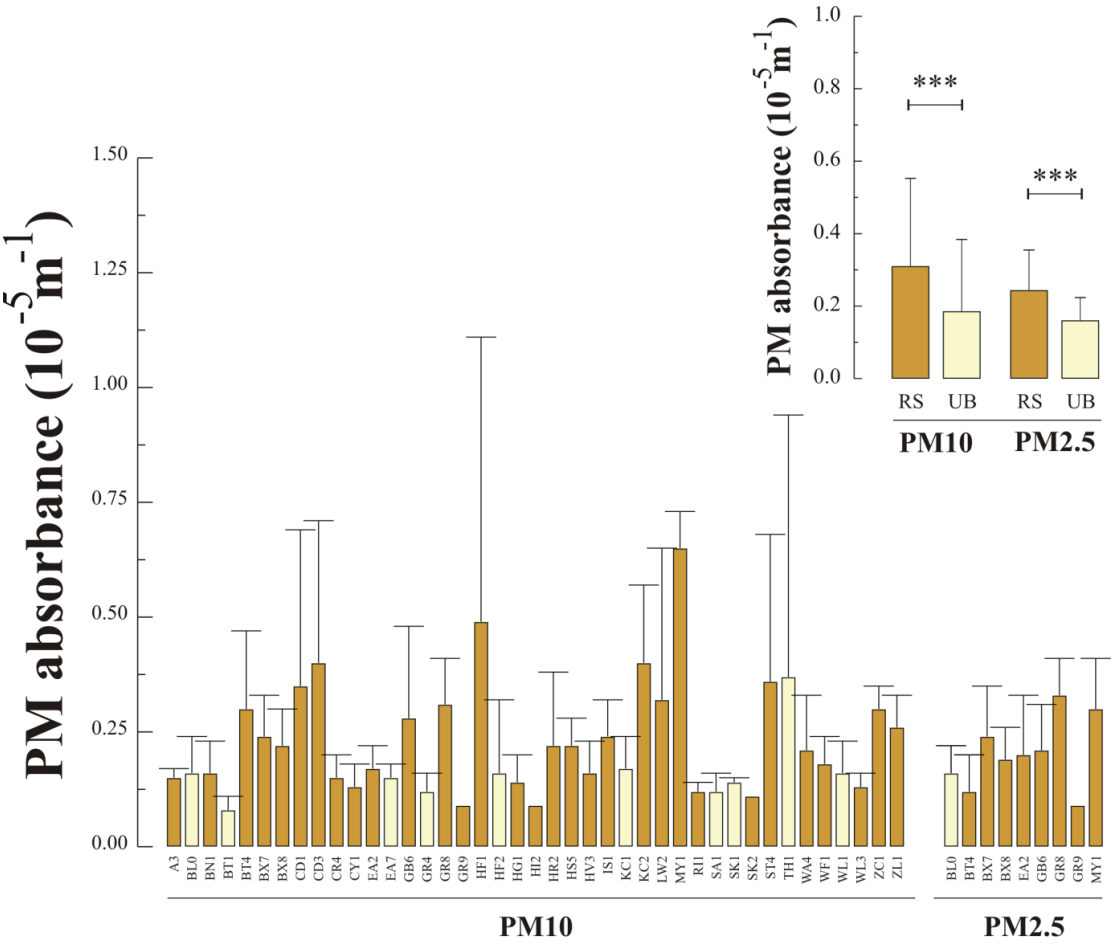


Figure B18. Summary of reflectance data for $PM_{10}$ and $PM_{2.5}$ filters.